ACS APPLIED NANO MATERIALS
Cite This: ACS Appl. Nano Mater. 2019, 2, 1102−1110
Article
www.acsanm.org

Dynamically Switching the Electronic and Electrostatic Properties of Indium−Tin Oxide Electrodes with Photochromic Monolayers: Toward Photoswitchable Optoelectronic Devices

Qiankun Wang,[†] Valentin Diez-Cabanes,[⊥] Simone Dell'Elce,[∥] Andrea Liscio,[∥,¶] Björn Kobin,[▽] Hong Li,[#] Jean-Luc Brédas,[#] Stefan Hecht,[▽] Vincenzo Palermo,[∥] Emil J. W. List-Kratochvil,[‡,§] Jérôme Cornil,[⊥] Norbert Koch,[*,†,‡] and Giovanni Ligorio[*,§]

[†]Institut für Physik and IRIS Adlershof, Humboldt-Universität zu Berlin, Brook-Taylor-Strasse 6, Berlin 12489, Germany
[‡]Helmholtz-Zentrum Berlin für Materialien und Energie GmbH, Albert-Einstein Strasse 15, Berlin 12489, Germany
[§]Institut für Physik, Institut für Chemie, and IRIS Adlershof, Humboldt-Universität zu Berlin, Brook-Taylor-Strasse 6, Berlin 12489, Germany
[⊥]Laboratory for Chemistry of Novel Materials, University of Mons, Place du Parc 20, Mons B-7000, Belgium
[∥]CNR-ISOF, Istituto per la Sintesi Organica e la Fotoreattività, Via P. Gobetti, Bologna 101-40129, Italy
[¶]CNR-IMM, Istituto per la Microelettronica e Microsistemi, Viale del Fosso del Cavaliere, Roma 110-00133, Italy
[▽]Institut für Chemie and IRIS Adlershof, Humboldt-Universität zu Berlin, Brook-Taylor-Strasse 2, Berlin 12489, Germany
[#]Center for Organic Photonics and Electronics and School of Chemistry and Biochemistry, Georgia Institute of Technology, 901 Atlantic Drive N.W., Atlanta, Georgia 30332-0400, United States

Supporting Information

ABSTRACT: The chemical modification of electrodes with organic materials is a common approach to tuning the electronic and electrostatic landscapes between interlayers in optoelectronic devices, thus facilitating charge injection at the electrode/semiconductor interfaces and improving their performance. The use of photochromic molecules for surface modification allows a dynamic control of the electronic and electrostatic properties of the electrode and thereby enables additional functionalities in such devices. Here, we show that the electronic properties of a transparent indium−tin oxide (ITO) electrode are reversibly and dynamically modified by depositing organic photochromic switches (diarylethenes) in the form of self-assembled monolayers (SAMs). By combining a range of surface characterization and density functional theory calculations, we present a detailed picture of the SAM binding to ITO, the packing density of molecules, their orientation, and work function modification of the ITO surface due to SAM deposition. Upon illumination with UV and green light, we observe a reversible shift of the frontier occupied levels by 0.7 eV and concomitantly a reversible work function change of ca. 60 meV. Our results prove the viability of dynamic switching of the electronic properties of the electrode with external light stimuli upon modification with a monolayer of photochromic molecules, which could be used to fabricate ITO-based photoswitchable optoelectronic devices.

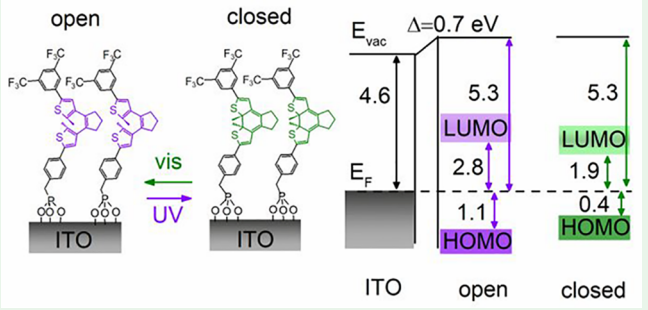

KEYWORDS: *photochromic switch, diarylethene, self-assembled monolayer, indium−tin oxide, interface electronic properties*

1. INTRODUCTION

The deposition of chemisorbed self-assembled monolayers (SAMs) is a powerful and universal approach to fine-tuning the desired electronic and electrostatic properties at surfaces and interfaces.[1−3] As a result of SAM formation, molecules are covalently bonded to the surface in an ordered manner and form a homogeneous coating with controlled molecular-height thickness. When (i) the deposited molecules possess a permanent dipole moment or (ii) chemisorption leads to a change of the surface electrostatic potential, this 2D array of molecules allows tuning of the surface potential in a wide range compared to other chemical modification techniques, e.g., surface etching,[4] plasma treatment.[5,6] Consequently, the interfacial energy-level alignment with regard to charge injection as well as extraction can be optimized by the deposition of SAMs.[1,7]

Received: January 16, 2019
Accepted: January 23, 2019
Published: January 23, 2019

DOI: 10.1021/acsanm.9b00094
ACS Appl. Nano Mater. 2019, 2, 1102−1110

On the other hand, the incorporation of photochromic or thermochromic molecules [e.g., diarylethenes (DAEs), azobenzenes, or dihydropyrenes] into the SAM provides a dynamic method to switch either the electronic and electrostatic properties or surface chemical properties through external stimuli such as light or temperature.[8−11] The underlying mechanism is that such molecules can switch reversibly between two isomeric configurations upon illumination at different wavelengths or upon heat absorption. Switching between the two isomers thereby fundamentally changes the electronic properties of the molecules, e.g., their electron affinity,[12] ionization potential,[13] and dipole moment.[14] Thus, with such physical−chemical properties, photochromic SAMs are expected to influence the development of multifunctional devices.[8,15] Among the families of photoswitches, DAEs are able to undergo a reversible change of the molecular conjugation (i.e., ring opening/closure reaction) upon light illumination. DAEs are extensively employed as photochromic systems because of their advantages of higher fatigue resistance and thermal stability in both isomeric states.[16,17] DAE-based SAMs were employed recently to modify metal electrodes[9] and proved to be able to optically modulate the current in organic field-effect transistors by changing the energy barriers at the metal/DAE interface. We recently demonstrated that DAE molecules functionalized with a phosphonic acid (PA) anchoring group can also be successfully employed for dynamic modification of the surface of a metal oxide such as ZnO.[18] It is therefore expected that such DAE SAMs will have similar effects on indium−tin oxide (ITO), a material relevant to electronic technologies, which has been extensively used as a transparent electrode in optoelectronic devices.

In this contribution, we investigate the hybrid interface resulting from the deposition on ITO of PA-DAE as SAMs. In particular, we demonstrate that the electronic properties of ITO can be dynamically and reversibly tuned by switching PA-DAE between its open and closed forms (the chemical structures of the two isomers are reported in Figure 1). Following our previous deposition methodology, which ensures a high-density coverage,[3,18] the PA-DAE SAM was deposited on the transparent electrode, and its modified surface was characterized by scanning force microscopy (SFM) and water contact angle. The chemical bonding of the PA anchoring group was assessed by measuring O 1s core-level spectra by means of X-ray photoemission spectroscopy (XPS). The orientation of the PA-DAE molecules on the surface was characterized by X-ray absorption spectroscopy (XAS). The work function modification and valence-electron properties were studied by ultraviolet photoemission spectroscopy (UPS). Upon illumination of the SAM, we observe a reversible shift of the frontier occupied levels by ca. 0.7 eV and concomitantly a small change in the work function by ca. 60 meV. Such light-induced experimental observations (i.e., frontier-level shift and work function change) are further substantiated at the density functional theory (DFT) level. Our findings establish the feasibility of dynamical energy level tuning on ITO electrodes, which could be used to fabricate multifunctional optoelectronic devices based on PA-DAE-modified ITO electrodes.

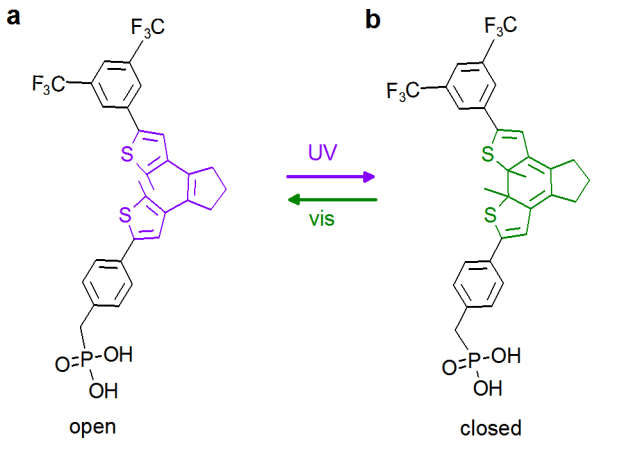

Figure 1. Chemical structure of the PA-DAE molecule with its (a) open and (b) closed forms, respectively. Upon illumination with UV and visible light, PA-DAE undergoes reversible photoswitching between its open and closed forms.

2. METHODS

ITO-coated glasses (sheet resistance = 20 Ω/□; purchased from Thin Film Devices Inc.) were precleaned by normal sonication procedures in acetone and isopropyl alcohol, respectively. The synthesis of PA-DAE molecules is reported in ref 18. The deposition of PA-DAE onto ITO is based on a procedure that has been optimized for PAs and extensively reported previously[3,18] and is as follows: the SAM was fabricated by immersion of the ITO-coated glass into a 1 mM solution of the PA-DAE switch (in the open form) in anhydrous tetrahydrofuran (THF) for 2 h and subsequently annealed in air for 40 min on a hot plate at 90 °C. Afterward, sonication in THF for 30 min was carried out to minimize the amount of physisorbed molecules. This preparation procedure was repeated three times in order to achieve a high density of PA-DAE.

Water-contact-angle measurements were performed with a Theta Lite (LOT-Oriel GmbH & Co. KG, Darmstadt, Germany) setup. The captured images were fitted by a Young−Laplace method to determine the contact angle. Sheet resistance values were obtained using a Jandel four-point probe setup with a RM3000 source measure unit. UV−vis absorption was measured with a PerkinElmer Lambda 950 spectrometer.

Photoemission spectroscopy (PES) and XAS were performed at the SurICat end station of Beamline PM4 at BESSY II. For PES, photoelectrons were collected with a hemispherical electron energy analyzer in normal emission geometry. The P 2p, C 1s, and O 1s core-electron regions were measured with photon energies of 265, 390, and 640 eV, respectively. In this way, the kinetic energy of the photoelectrons was kept at ca. 100 eV in order to probe a similar sample depth and maximize the surface sensitivity. The binding energies of the core electrons were referenced to the Au $4f_{7/2}$ level (84.0 eV). The valence- and core-electron regions were characterized with He I ($h\nu$ = 21.2 eV, with an Al-foil filter) and Al Kα ($h\nu$ = 1486.6 eV) lines, respectively, in a custom-made system. The secondary electron cutoff (SECO) spectra were recorded with samples biased at −10 V. The Fermi level is referred to as the zero binding energy in all UPS and XPS spectra. Spectra were fitted with both symmetric Voigt and asymmetric Doniach-Sunjic (e.g., for ITO O 1s) profiles after subtracting a Shirley background. XAS experiments were carried out in the total electron yield mode. The incident beam was horizontally polarized, and the degree of linear polarization was determined to be 0.9. The sample currents were measured using a Keithley 6514 electrometer via a double-shielded BNC cable. The sample surface morphology was measured using a scanning force microscope equipped with a Bruker Dimension FastScan system in tapping mode. Height and phase images were recorded using Al-coated silicon probes with a spring constant of 0.4 N m^{-1}. This instrument was also used for Kelvin probe force microscopy (KPFM) investigations using SCM-PIT probes. The cantilever spring constant is 2.8 N m^{-1}. Relevant SFM and KPFM data were evaluated using the *Gwyddion* program.

DOI: 10.1021/acsanm.9b00094
ACS Appl. Nano Mater. 2019, 2, 1102−1110

In order to trigger the switching process, the samples were irradiated in situ during UPS measurements through a viewport of the analysis chamber with green (λ centered at 565 nm) or UV (λ centered at 365 nm) light, which were provided by high-power light-emitting diodes (Thorlabs) mounted with an adjustable collimator. The measured maximum photon intensities were ca. 200 mW cm^{-2} for green light and 100 mW cm^{-2} for UV light, respectively.

In the case of DFT calculations, the building of the ITO surface within a slab approach has been reported previously in the literature.[19−21] The unit cell consists of three (In−O)/(Sn−O) layers with an In/Sn ratio of 0.14. All O atoms belonging to the top layer of the ITO slab are saturated with H atoms to model a realistic OH-terminated surface, while the bottom layer is not passivated. The surface unit-cell dimensions are a = 24.79 Å and b = 14.32 Å; a vacuum region of 32 Å is set in the normal direction to the slabs, with a dipole correction layer introduced into middle (Figure S1).[22] This vacuum region is large enough to ensure convergence of the dipole moment in the normal direction (Figure S2). Four PA-DAE molecules (n = 4) in the open or closed forms were attached to the ITO surface. Note that adsorption of the PA-DAE molecules is not accompanied by any loss of atoms from the ITO surface; however, the H atoms belonging to the PA group are released upon deposition of the SAM. The O atoms of the PA groups are connected to both OH groups and In/Sn atoms from the ITO surface (Figure S1). The resulting surface area is A = 88.75 Å^2 per molecule. This value is higher than the experimental one obtained by XPS, which is A = 50 ± 11.54 Å^2 per molecule. This difference has no major implications in view of a recent work of Li et al. on a (trifluorophenyl)phosphonic acid SAMS on ITO, showing that, in the high coverage regime (n = 4) of the same unit cell, the value of $\Delta\phi$ has already converged within 0.1 eV compared to the value obtained with the experimental coverage.[19] The unit-cell optimizations were performed at the DFT level with the Perdew−Burke−Ernzerhof (PBE) exchange-correlation functional[23] within the gradient generalized approximation using the plane-augmented-wave method,[24] as implemented in the Vienna Ab-initio Simulations Package (*VASP*) code. The plane-wave cutoff was set at 300 eV, and a value of 10^{-6} eV was chosen for the total energy convergence; a k sampling of 2 × 2 × 1 and the tetrahedron integration method were used in the Brillouin zone. Geometry optimizations were carried out following a damped molecular dynamics method with a force cutoff for the convergence equal to 0.04 eV Å^{-1}. In order to decrease the computational time, the coordinates of the bottom two (In−O)/(Sn−O) layers were frozen during the optimizations.

3. RESULTS AND DISCUSSION

3.1. Surface Morphology. The surface morphologies of the bare ITO and PA-DAE-modified ITO were characterized by SFM (Figure 2). For the bare ITO, the height image (Figure 2a) of the surface shows small grains (average size of ca. 40 nm diameter) with a roughness (root-mean-square) of 0.7 ± 0.1 nm. Upon SAM deposition, the surface roughness does not change significantly (0.4 ± 0.1 nm); the ITO grains are preserved, and no island formation or multilayers are observable in the height image (Figure 2b). Combining the height and (homogeneous) phase images (Figure 2c,d) allows us to conclude that surface modification results in uniform coverage. In order to characterize the SAM-modified ITO, we investigated the wettability change induced by PA-DAE by means of a contact-angle measurement before and after SAM deposition (water was used as the test liquid). The contact angle of water increases significantly from 33.1 ± 1.0° on clean ITO to 97.1 ± 1.0°, as expected from the induced hydrophobic properties of the F head groups attached to DAE. The results are consistent with the observation for the PA-DAE SAM on ZnO (where the water contact angle increases from 46° to 101°).[18] Such a wettability change also points toward densely

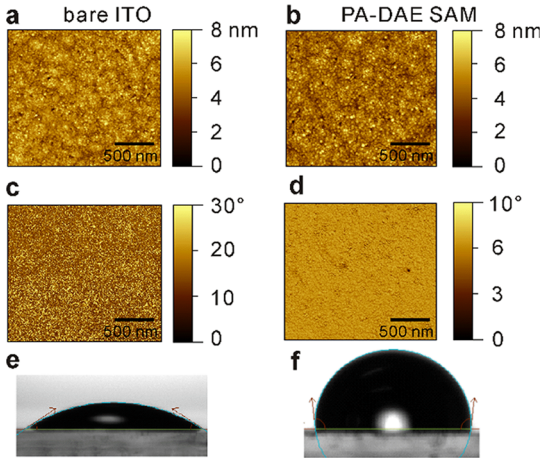

Figure 2. SFM height and phase images for bare ITO (a and c) and ITO with PA-DAE SAM (b and d) surfaces. Water contact angles of the corresponding surfaces are shown for the (e) bare ITO and (f) SAM, respectively.

packed coverage on the ITO surface.[3,25] It is worth mentioning that upon SAM modification neither the sheet resistance of ITO (measured with a four-point probe) nor its transparency (measured via UV−vis absorption) was influenced.

3.2. Chemical Bonding. To further verify the quality of the SAM films and to confirm chemisorption of the anchoring group of the switching molecules onto ITO, we performed XPS measurements with synchrotron radiation. This enables us to tune the photon energy for photon excitation to ensure a minimal escape depth of the measured electrons and thus achieve the highest surface sensitivity possible with this technique. The beam damage on the organic molecules during measurement can be neglected by analyzing the C 1s spectra (Figure S3 and Table S1). The P 2p core-level peak was first measured to ensure the presence of PA (Figure 3a). On the bare ITO surface (bottommost spectra), no signal can be detected; however, after surface modification (topmost spectra), the P 2p peak is clearly observed, and two components are resolved from the fitting of the spectra. The

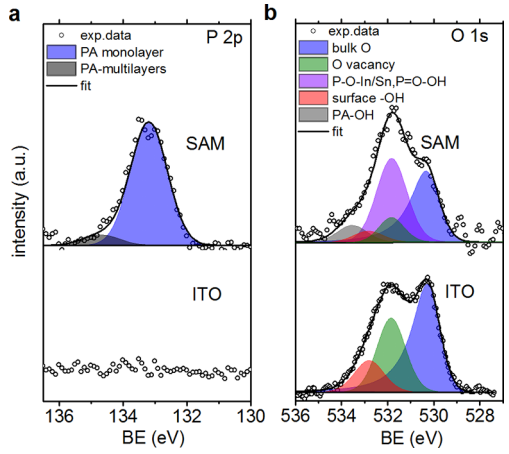

Figure 3. P 2p (a) and O 1s (b) core-level spectra for bare ITO (bottom) and ITO with PA-DAE SAM (top). Decomposition of the P 2p spectra shows that PA-DAE molecules primarily form a monolayer; and decomposition of the O 1s spectra reveals the chemical nature of the PA bonding to ITO.

DOI: 10.1021/acsanm.9b00094
ACS Appl. Nano Mater. 2019, 2, 1102−1110

component at 133.2 eV binding energy is attributed to the chemisorbed PA-DAE monolayer.[3] The additional component at higher binding energy (135.0 eV) is attributed to the presence of a small amount of physisorbed molecules (8.0% with respect to the chemisorbed molecules). The packing density of the PA-DAE molecules is analyzed by comparing the signal intensity of F 1s with that of In 3d (Figure S4 and eq S1), thus yielding ca. 2.0 ± 0.7 molecules nm^{-2}. The result is comparable to previous observations for PA-DAE on ZnO.[18]

The O ls core-level spectra were measured to investigate the nature of the chemical bonding between the PA-DAE and ITO. Figure 3b displays the O 1s spectra before (bottommost) and after (topmost) PA-DAE modification. For bare ITO, three spectral components are resolved. Following earlier DFT calculations,[26] the two components at lower binding energy are attributed to (i) ITO bulk oxygen (at 530.3 eV; the peak is asymmetric because of energy loss) and (ii) surface oxygen vacancy (at 531.8 eV). The third resolved component is located at 532.8 eV and attributed to the adsorbed surface hydroxyl groups.[27] After SAM deposition, the O 1s intensity from bulk ITO is markedly attenuated, and the feature at ca. 531.7 eV (1.4 eV higher than the binding energy of bulk oxygen) in the spectral signal increases in intensity. The fitting of the spectrum suggests that an additional component has to be considered in order to justify the intensity modification in this region; this additional peak arises from chemisorption of the PA anchoring group. In our previous studies, it was established that chemisorption of PA-DAE on ZnO surfaces occurs in both the bidentate and tridentate binding modes.[18] We thus tentatively attribute the PA peak to the coexistence of bidentate and tridentate coordination on ITO.

To support the assignment of the new O 1s peak and to elucidate the binding mechanism between PA-DAE and ITO, DFT calculations were performed to estimate the O 1s core-level shift. On the basis of the literature,[19,28,29] the coexistence of both bidentate and tridentate binding modes in DFT calculations has been considered with a 1:1 ratio. Here, after optimization of the unit cell (Figure 4a,b), sites 1 and 3 are found to display a bidentate binding with two PA O atoms bonded to Sn/In atoms and another O atom in electrostatic interaction with an ITO surface hydroxyl group; sites 2 and 4 exhibit tridentate binding, with the three O atoms of PA bonded to surface Sn and In atoms. The core-level shift of the O 1s belonging to the PA groups was calculated in the final-state approximation.[30,31] The calculated core-level shift of PA with respect to the binding energy of bulk oxygen is shown in Figure 4c. Among the four adsorption sites, we find that the core-level binding energies are not highly affected whether the O atom is electrostatically connected to the hydroxyl groups in the bidentate mode or bonded to ITO Sn/In atoms; the majority of the values lie between 1.2 and 1.3 eV for both bidentate and tridentate modes. These values are in quantitative agreement with the XPS data (1.4 eV) discussed in Figure 3b, which points to the fact that bidentate and tridentate modes most likely coexist and are not energetically resolved. Therefore, using the bulk oxygen binding energy from the bare ITO as a reference (530.3 eV from XPS), one peak at ca. 531.7 eV should be added to the peak fitting made in Figure 3 to account for the coexistence of bidentate and tridentate binding. The values of the O 1s core-level shifts for PA bindings are also in good agreement with the literature observations for alkyl- and arylphosphonic acid SAMs adsorbed on ITO.[25,32] In addition, no clear changes in the

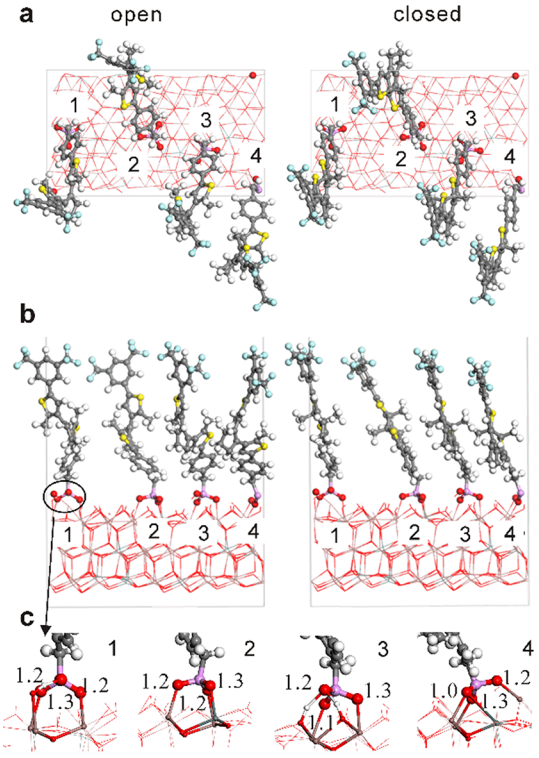

Figure 4. Top (a) and lateral (b) views of the ITO unit cells with a PA-DAE SAM in the open (left) and closed (right) isomeric forms. The figure illustrates the two bidentate (sites 1 and 3) and tridentate (sites 2 and 4) binding modes as well as the zoom on the PA binding to ITO for the four different adsorption sites (c); the values (in eV) reported in part c correspond to the DFT-calculated O 1s binding energy shifts with respect to the O atoms in bulk ITO.

core-level shifts are observed in the DFT calculations when going from the open to closed forms (see Table S2), which implies that photoswitching of the SAM does not impact the PA bonding strength.

3.3. Orientation of the SAM. Angle-dependent XAS was performed to measure the orientation of the PA-DAE molecules once the SAM is formed on ITO. As shown in Figure 5a, the spectra were collected from the C K-shell

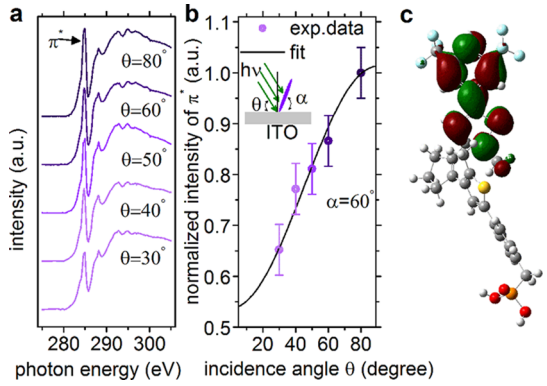

Figure 5. Angle-dependent C K-edge XAS (a) of the PA-DAE SAM on ITO. Plots of the π^*-orbital intensities as a function of the photon incidence angle θ (b). The solid curve corresponds to the best fit of the intensity evolution indicated with a tilt angle of 60° for PA-DAE. Molecular orbitals for the excited state corresponding to the first π resonance of the C atoms (c).

DOI: 10.1021/acsanm.9b00094
ACS Appl. Nano Mater. 2019, 2, 1102−1110

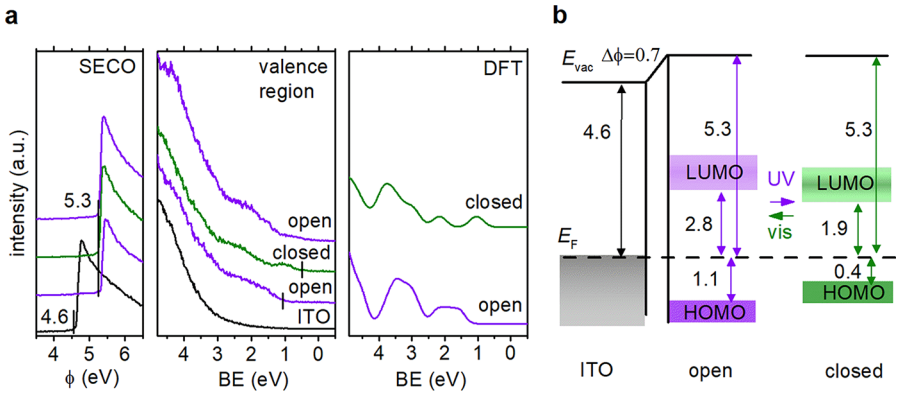

Figure 6. Evolution of the work function (a, left) and valence-electron region (a, center) of ITO upon deposition of the PA-DAE SAM. The figures report the induced changes upon illumination with UV and visible light. The DFT-calculated DOSs for PA-DAE for the open and closed isomers are also plotted for comparison (a, right). Schematic energy-level diagram at the ITO/PA-DAE interface (b). The energy positions of the vacuum (E_{vac}) and HOMO levels are derived from UPS, while the LUMO level of PA-DAE is calculated using the transport gap of related DAE derivatives.[8]

electrons excited to unoccupied molecular orbitals. The most intense transition located at 285.0 eV exhibits a strong angular dependence and is assigned to C 1s → π^* orbital transitions. Because the C 1s initial state of C is spherically symmetric and bears no angular momentum, the angular dependencies of the absorption intensity will be directly dependent on the π^*-orbital orientation in the final state. For the open form, the lowest unoccupied π^* molecular orbitals are perpendicular to the top phenyl plane (shown in Figure 5c). To quantify the average orientation of PA-DAE in the SAM, the intensity of π^* (I_{π^*}) was measured at five different angles between the incoming polarized light and the sample normal. The molecular tilt angle α (with respect to the ITO surface; see the inset of Figure 5b) is calculated as the best fit according to eq S2 (for details, see the Supporting Information). The average tilt angle is thus calculated to be $\alpha = 60°$. Because the molecular orientation in the monolayer is strongly dependent on the molecule−substrate and molecule−molecule interactions as well as on the molecular packing details,[21,29] such results are reasonable compared to other fluorinated alkyl- and benzylphosphonic acids on ITO.[20,21,29] The measured tilt angle is further supported by the DFT results, which indicate that, for the geometrically relaxed monolayer on ITO, PA-DAE displays an average angle of ca. 58° with respect to the surface in both the open and closed forms (see Table S3 and Figure S5 for tilt angle details).

3.4. Electronic Properties of the SAM. UPS measurements were performed to investigate the changes induced by PA-DAE on the valence-electron properties of ITO. Figure 6a shows the UPS spectra of the bare ITO and with PA-DAE modification; the latter sample was measured immediately after SAM deposition, and thus PA-DAE was initially in the open form. The work function (ϕ) of the bare ITO was determined by measuring the SECO region and amounts to 4.6 eV (see the leftmost panel in Figure 6a). Modification with the PA-DAE SAM increases ϕ by 0.7 eV up to 5.3 eV. The valence-electron region (central panel) also displays a modification in the density of states (DOS) upon SAM deposition. The UPS spectra exhibit a structure assigned to the highest occupied molecular orbital (HOMO) of open PA-DAE (PA-DAE-o), with the onset measured at 1.1 eV binding energy. Thus, the ionization potential (calculated as the sum of SECO and HOMO) is 6.4 eV, in good agreement with the previous results on ZnO.[18] The SAM was subsequently illuminated in situ (for 60 s) with UV light to induce a photoswitching from the open to closed form (PA-DAE-c). The induced PA-DAE-c isomer displays increased molecular conjugation (Figure 1), which translates into the appearance of a feature at lower binding energy than the HOMO of molecules in the open configuration. Thus, this feature is the PA-DAE-c HOMO with an onset at 0.4 eV. Subsequent illumination of the SAM with green light for 120 s reversibly switches PA-DAE to its open form, as evidenced by the disappearance of the PA-DAE-c HOMO and reappearance of the PA-DAE-o valence-electron features.

To assess the valence-electron features, the DOSs of isolated PA-DAE were computed for both the open and closed forms and broadened with Gaussian functions (the eigenvalues are convoluted by a Gaussian function with a full width at half-maximum of 0.4 eV to be consistent with the UPS resolution). The calculated DOS is in excellent agreement with the UPS data (see the rightmost panel in Figure 6a) and confirms the experimental observation of the HOMO energy shift upon photoswitching between the isomers.

Interestingly, no work function changes are observed for both the SAM (Figure 6) and ITO (Figure S6) surfaces. Therefore, to better assess the work function modification upon switching, the surface potential of the SAM was measured with KPFM. A reversible switching of the surface potential is observed upon UV- and green-light illumination cycles (Figures S7 and S8). Such a reversible potential change results from photoswitching of the SAM because illumination on bare ITO surfaces induces smaller than 10 meV potential variances (Figure S8). In particular, the PA-DAE-c surface potential turns out to be ca. 60 ± 5 meV higher than the PA-DAE-o surface potential. Similar switching-induced potential changes have been observed in other DAE SAMs on metal by KPFM.[9] We note that the reason why UPS does not resolve such a small potential change can presumably be attributed to (i) a possible charging effect during UPS measurements and (ii) UV-induced photodegradation of the SAM;[33] the latter would give rise to a relatively poor switching yield, with the measured work function then likely arising from a superposition of the open and closed forms.

The KPFM potential change can be directly attributed to the change in the PA-DAE dipole moment (μ) upon switching. It is useful at this stage to revisit the packing density (n) of the

DOI: 10.1021/acsanm.9b00094
ACS Appl. Nano Mater. 2019, 2, 1102−1110

SAM molecules, which can be estimated according to the Helmholtz equation:[34]

$$(\Delta\phi)_{o-c} = \frac{en(\Delta\mu)_{o-c}\sin(\alpha)}{\varepsilon_r\varepsilon_0} \quad (1)$$

where $(\Delta\phi)_{o-c}$ is the KPFM potential change upon switching, i.e., 60 meV, e is the elementary charge, α is the molecular tilt angle as derived from XAS, and $(\Delta\mu)_{o-c}$ is the dipole moment difference between the open and closed forms for the isolated molecules. According to our previous calculations on isolated molecules,[18] $(\Delta\mu)_{o-c}$ is 0.2 D; however, it should be noted that a high molecular coverage (typically for complete or quasi-complete monolayers) not only increases the density of the dipoles but also enhances the depolarization effect of the surrounding dipoles.[35] This can be accounted for by a relative dielectric constant ε_r of ca. 1.5.[3,19] The packing density n thus turns out to be 1.5 ± 0.3 molecules nm^{-2}, as calculated with eq 1, in good agreement with the value of 2.0 ± 0.7 molecules nm^{-2} estimated from XPS, as discussed above.

We summarize in Figure 6b the energy-level alignment for ITO functionalized with the PA-DAE SAM. The values of the relative energy separation between the Fermi (E_F), HOMO, and vacuum levels are derived directly from UPS, while the lowest unoccupied molecular orbital (LUMO) energy is obtained by referring to the transport gap of DAE derivatives measured by inverse PES.[12] Upon SAM deposition, the work function increases with a consequent upshifting of the vacuum level; this is attributed to the formation of interface dipoles, as discussed below. Similar to the observations made on ZnO, PA-DAE can be used to optically control and modulate the hole injection barrier because the energy difference between HOMO and E_F is reversibly modulated upon illumination with light (i.e., 1.1 and 0.4 eV for the open and closed forms, respectively). In parallel, the LUMO-to-E_F energy difference decreases from 2.8 to 1.9 eV upon going from the open to closed forms. Thus, the HOMO and LUMO energy differences between the open and closed forms are $\Delta E_{o\text{-}c,HOMO}$ = 0.7 eV and $\Delta E_{o\text{-}c,LUMO}$ = 0.9 eV, respectively.

In order to further understand the relative energy-level alignment between the two isomers, we have also calculated at the DFT level the frontier-level evolution of PA-DAE upon going from the isolated molecule to the packed monolayer. In the isolated molecules, the HOMO [LUMO] of PA-DAE-c is located at higher [lower] energy than that of PA-DAE-o because of the increase in conjugation and the resulting band-gap reduction in the closed form (Table S5); the calculated $\Delta E_{o-c,HOMO}$ and $\Delta E_{o-c,LUMO}$ are both 0.7 eV. When the calculated coverage is increased up to a full monolayer, all frontier molecular orbital energies exhibit an upward shift by ca. 0.3 eV (Figure S9) because of the intermolecular interactions; this shift saturates at a degree of coverage n = 3 (i.e., three molecules per unit cell). However, the relative energy-level alignment remains preserved; i.e., $\Delta E_{o-c,HOMO}$ = 0.5 eV and $\Delta E_{o-c,LUMO}$ = 0.9 eV. After deposition on the ITO surface, the interaction of the SAM with the ITO surface does not significantly affect this relative alignment, with calculated values of $E_{o-c,HOMO}$ = 0.8 eV and $\Delta E_{o-c,LUMO}$ = 0.6 eV (Figure S10).

3.5. Theoretical Understanding of the Surface Potential Change. To shed light on the surface potential modification at the ITO/PA-DAE interface, we performed theoretical modeling at the DFT level. The isolated PA-DAE molecules were first geometrically optimized with the PBE functional,[23] and four PA-DAE molecules were subsequently grafted onto the ITO surface (in both tridentate and bidentate binding modes); the resulting unit cell was then optimized, as described in the Methods section. The work function modification, defined as the work function difference ($\Delta\phi$) between the SAM-modified ITO ($\phi_{ITO/SAM}$) and bare ITO (ϕ_{ITO}), can be decomposed into three contributions:[19,36,37]

$$\Delta\phi = \phi_{ITO/SAM} - \phi_{ITO} = V_{BD} + V_{\mu SAM} + V_{Relax\text{-}ITO} \quad (2)$$

where V_{BD} represents the creation of a bond dipole at the ITO/PA-DAE interface due to charge reorganization upon SAM formation, $V_{\mu SAM}$ is linked to the intrinsic dipole of PA-DAE in the monolayer, and $V_{Relax\text{-}ITO}$ is the work function change of ITO due to surface geometry relaxation upon SAM grafting. In order to quantify the first term V_{BD} in eq 2, Poisson's equation $\nabla^2 V(z) = -\Delta\rho(z)/\varepsilon_0$ is used and requires evaluation of the charge-density difference $\Delta\rho(z)$. The latter is calculated in the so-called "molecular scenario" as[38,39]

$$\Delta\rho(z) = \rho_{ITO/SAM}(z) - \rho_{ITO}(z) - \rho_{PA\text{-}DAE\text{-}H}(z) + \rho_H(z) \quad (3)$$

where $\rho_{ITO/SAM}$ denotes the plane-averaged charge density of the full ITO/SAM system, ρ_{ITO} the charge density of the relaxed ITO surface, $\rho_{PA\text{-}DAE\text{-}H}$ the charge density of the PA-DAE layer with H atoms added to recover the neutral PA-DAE molecule, and ρ_H the charge density of the isolated H atoms in the same location as in the neutral PA-DAE SAM. The calculations were independently performed with both open and closed isomer configurations. Figure 7 displays $\Delta\rho(z)$ and its cumulated charge reorganization [$\Delta Q(z) = \int \Delta\rho(z)\, dz$] upon SAM formation along the z axis (taken as the direction normal to the surface).

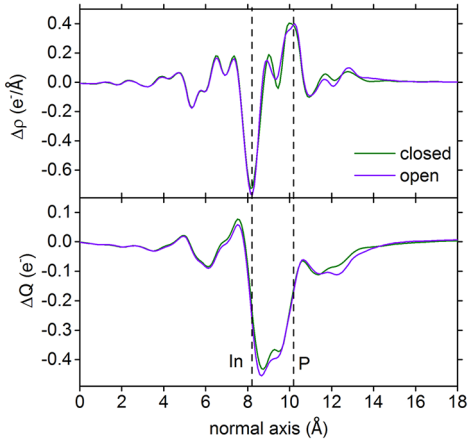

Figure 7. Plane-averaged charge-density difference (top) and charge transfer (bottom) at the ITO/PA-DAE interface for the open and closed forms. The vertical dashed lines denote the averaged position of the top layer In and P atoms.

The calculations show that $\Delta\rho$ exhibits a similar distribution for both the open and closed forms and that the amount of charge transferred (ΔQ) from ITO to PA-DAE has the same magnitude. A Bader population analysis[40] indicates that the amount of charge transfer is 1.36|e| per PA-DAE molecule (Table S4). The transferred charge is mostly localized within the PA anchoring group (−1.26|e|), while the charges in the DAE backbone are only slightly modified (−0.1|e|). Estimation

DOI: 10.1021/acsanm.9b00094
ACS Appl. Nano Mater. 2019, 2, 1102−1110

of the molecular dipole contribution of the SAM to $\Delta\phi$ ($V_{\mu SAM}$) is made from the isolated monolayer of PA-DAE molecules (i.e., nonbonded to the ITO surface) while retaining the same molecular geometry as that in the SAM bonded to ITO (H atoms were added to keep the system neutral). The plane-averaged electrostatic potential was computed across the SAM layer. The third term in eq 2 is related to the nuclear relaxation effect in ITO ($V_{Relax\text{-}ITO}$) upon SAM formation; it is evaluated as the difference $V_{Relax\text{-}ITO} = \phi_{ITO}' - \phi_{ITO}$ between the work function of the pristine ITO surface (ϕ_{ITO}) and the work function of the ITO surface without any SAM but in the geometry that it adopts upon SAM grafting (ϕ_{ITO}'). The work function change and its three components are summarized in Table 1. For both open and closed SAMs, the values of V_{BD} are

Table 1. Decomposition of the ITO Work Function Modification ($\Delta\phi$) into Its Three Components According to DFT[a]

	V_{BD}	$V_{\mu SAM}$	$V_{Relax\text{-}ITO}$	$\Delta\phi = \sum_i V_i$
open	0.61	1.29	−0.42	1.48
closed	0.55	1.57	−0.41	1.71
$\phi_{ITO/SAM}$		ϕ_{ITO}	$\Delta\phi = \phi_{ITO/SAM} - \phi_{ITO}$	
4.68		3.20	1.48	
4.92		3.20	1.72	

[a] $\Delta\phi$ is calculated according to $\Delta\phi = V_{BD} + V_{\mu SAM} + V_{Relax\text{-}ITO} = \phi_{ITO/SAM} - \phi_{ITO}$ (eq 2). All quantities are defined in the text and are given in electronvolts.

compensated for by $V_{Relax\text{-}ITO}$ ($V_{BD} + V_{Relax\text{-}ITO} \approx 0.2$ eV), thus making the magnitude of $\Delta\phi$ primarily driven by the molecular dipole component $V_{\mu SAM}$. The DFT-calculated $\Delta\phi$ for the closed form is ca. 200 meV higher than that of the open form, which is consistent with the KPFM results (60 meV). This $\Delta\phi$ difference between the open and closed forms is mainly ascribed to a higher value of the molecular contribution ($V_{\mu SAM}$) in the closed form. A further theoretical analysis of the PA-DAE dipole magnitude as a function of the coverage (Figure S11 and Table S6) illustrates that the difference in $V_{\mu SAM}$ between the open and closed forms is slightly reduced with an increase in the degree of coverage because of the different extents of depolarization effects between the two forms.[35] Although the relative changes in $\Delta\phi$ are well reproduced by the calculations, it has to be emphasized that the absolute value of the theoretical $\Delta\phi$ is twice as large as the experimental value (0.7 eV). We suggest that this discrepancy is likely related to a Fermi-level pinning effect of the molecular levels, which creates another interfacial dipole contribution. This process appears not to be well depicted by the DFT calculations, and two reasons can be put forward for this: (i) the relative energy-level alignment of the isolated components (ITO versus PA-DAE molecules) is not adequately described and/or (ii) much larger unit cells are needed to describe a full charge transfer between the molecule and electrode to properly describe the Fermi-level pinning. Fully addressing this issue is, however, beyond the scope of the present work.

4. CONCLUSIONS

In summary, we have demonstrated the possibility of controlling and optically modulating the electrostatic potential landscape (and, thus, the electronic energy-level alignment) at interfaces with ITO, one of the most widely utilized transparent conductive oxides. For this purpose, the bare surface of ITO was functionalized with a SAM of photochromic diarylethene molecules (functionalized with PA as the anchoring group). The PA-DAE SAM was comprehensively investigated by contact-angle, SFM, XPS, XAS, and UPS measurements. The combination of these characterizations provides a detailed picture of the coverage (ca. 1.5 molecules nm^{-2}), chemical binding (coexistence of bi- and trifold binding between the phosphonic group and ITO), and arrangement of PA-DAE SAMs on the substrate (tilt angle of 60°). Both XPS and UPS data are further supported by the DFT results. When illumination of UV and green light is alternated, the PA-DAE molecule switches between the open and closed isomeric configurations. This leads to reversible frontier-level energy shifts (0.7 eV for HOMO and 0.9 eV for LUMO) as well as to a small work function change (60 meV), evolutions that are fully consistent with the DFT results. Our findings thus provide a pathway to modify the electrode surface electronic properties upon external light illumination, and this strategy will be further employed in ITO-based photoswitchable devices.

■ ASSOCIATED CONTENT

Supporting Information

The Supporting Information is available free of charge on the ACS Publications website at DOI: 10.1021/acsanm.9b00094.

Unit cell of PA-DAE on ITO, C 1s core-level spectra, quantification of the PA-DAE packing density, quantification of the PA-DAE orientation, PA-DAE KPFM image, and DFT data of the PA-DAE frontier levels (PDF)

■ AUTHOR INFORMATION

Corresponding Authors

*E-mail: nkoch@physik.hu-berlin.de.
*E-mail: giovanni.ligorio@hu-berlin.de.

ORCID

Jean-Luc Brédas: 0000-0001-7278-4471
Stefan Hecht: 0000-0002-6124-0222
Emil J. W. List-Kratochvil: 0000-0001-9206-800X
Jérôme Cornil: 0000-0002-5479-4227
Norbert Koch: 0000-0002-6042-6447
Giovanni Ligorio: 0000-0001-9277-6903

Author Contributions

The manuscript was written through contributions of all authors. All authors have given approval to the final version of the manuscript.

Funding

This work was financially supported by the EC through the Marie Curie Project ITN iSwitch (Grant 642196) and DFG (SFB 951). The work at Georgia Tech was supported by the Office of Naval Research under Award No. N00014-17-1-2208. Computational resources were provided by the Consortium des Équipements de Calcul Intensif funded by the Belgian National Fund for Scientific Research (FRS-FNRS) under Grant 2.5020.11. J.C. is an FNRS research director.

Notes

The authors declare no competing financial interest.

DOI: 10.1021/acsanm.9b00094
ACS Appl. Nano Mater. 2019, 2, 1102−1110

REFERENCES

(1) Paniagua, S. A.; Giordano, A. J.; Smith, O. L.; Barlow, S.; Li, H.; Armstrong, N. R.; Pemberton, J. E.; Bredas, J. L.; Ginger, D.; Marder, S. R. Phosphonic Acids for Interfacial Engineering of Transparent Conductive Oxides. *Chem. Rev.* **2016**, *116*, 7117−7158.

(2) Love, J. C.; Estroff, L. A.; Kriebel, J. K.; Nuzzo, R. G.; Whitesides, G. M. Self-Assembled Monolayers of Thiolates on Metals as a Form of Nanotechnology. *Chem. Rev.* **2005**, *105*, 1103−1169.

(3) Timpel, M.; Nardi, M. V.; Krause, S.; Ligorio, G.; Christodoulou, C.; Pasquali, L.; Giglia, A.; Frisch, J.; Wegner, B.; Moras, P.; et al. Surface Modification of ZnO(0001)-Zn with Phosphonate-Based Self-Assembled Monolayers: Binding Modes, Orientation, and Work Function. *Chem. Mater.* **2014**, *26*, 5042−5050.

(4) Wang, Z.; Dong, H.; Zou, Y.; Zhao, Q.; Tan, J.; Liu, J.; Lu, X.; Xiao, J.; Zhang, Q.; Hu, W. Soft-Etching Copper and Silver Electrodes for Significant Device Performance Improvement toward Facile, Cost-Effective, Bottom-Contacted, Organic Field-Effect Transistors. *ACS Appl. Mater. Interfaces* **2016**, *8*, 7919−7927.

(5) Zhou, Y.; Shim, J. W.; Fuentes-Hernandez, C.; Sharma, A.; Knauer, K. A.; Giordano, A. J.; Marder, S. R.; Kippelen, B. Direct Correlation between Work Function of Indium-Tin-Oxide Electrodes and Solar Cell Performance Influenced by Ultraviolet Irradiation and Air Exposure. *Phys. Chem. Chem. Phys.* **2012**, *14*, 12014−12021.

(6) Wu, C. C.; Wu, C. I.; Sturm, J. C.; Kahn, A. Surface Modification of Indium Tin Oxide by Plasma Treatment: An Effective Method to Improve the Efficiency, Brightness, and Reliability of Organic Light Emitting Devices. *Appl. Phys. Lett.* **1997**, *70*, 1348−1350.

(7) Lange, I.; Reiter, S.; Kniepert, J.; Piersimoni, F.; Pätzel, M.; Hildebrandt, J.; Brenner, T.; Hecht, S.; Neher, D. Zinc Oxide Modified with Benzylphosphonic Acids as Transparent Electrodes in Regular and Inverted Organic Solar Cell Structures. *Appl. Phys. Lett.* **2015**, *106*, 113302.

(8) Orgiu, E.; Crivillers, N.; Herder, M.; Grubert, L.; Pätzel, M.; Frisch, J.; Pavlica, E.; Duong, D. T.; Bratina, G.; Salleo, A.; et al. Optically Switchable Transistor via Energy-Level Phototuning in a Bicomponent Organic Semiconductor. *Nat. Chem.* **2012**, *4*, 675−679.

(9) Mosciatti, T.; del Rosso, M. G.; Herder, M.; Frisch, J.; Koch, N.; Hecht, S.; Orgiu, E.; Samorì, P. Light-Modulation of the Charge Injection in a Polymer Thin-Film Transistor by Functionalizing the Electrodes with Bistable Photochromic Self-Assembled Monolayers. *Adv. Mater.* **2016**, *28*, 6606−6611.

(10) Crivillers, N.; Osella, S.; Van Dyck, C.; Lazzerini, G. M.; Cornil, D.; Liscio, A.; Di Stasio, F.; Mian, S.; Fenwick, O.; Reinders, F.; et al. Large Work Function Shift of Gold Induced by a Novel Perfluorinated Azobenzene-Based Self-Assembled Monolayer. *Adv. Mater.* **2013**, *25*, 432−436.

(11) Bakkar, A.; Cobo, S.; Lafolet, F.; Saint-Aman, E.; Royal, G. A New Surface-Bound Molecular Switch Based on the Photochromic Dimethyldihydropyrene with Light-Driven Release of Singlet Oxygen Properties. *J. Mater. Chem. C* **2015**, *3*, 12014−12017.

(12) Wang, Q.; Frisch, J.; Herder, M.; Hecht, S.; Koch, N. Electronic Properties of Optically Switchable Photochromic Diarylethene Molecules at the Interface with Organic Semiconductors. *ChemPhysChem* **2017**, *18*, 722−727.

(13) Frisch, J.; Herder, M.; Herrmann, P.; Heimel, G.; Hecht, S.; Koch, N. Photoinduced Reversible Changes in the Electronic Structure of Photochromic Diarylethene Films. *Appl. Phys. A: Mater. Sci. Process.* **2013**, *113*, 1−4.

(14) Klajn, R. Spiropyran-Based Dynamic Materials. *Chem. Soc. Rev.* **2014**, *43*, 148−184.

(15) Gemayel, M. El; Börjesson, K.; Herder, M.; Duong, D. T.; Hutchison, J. a; Ruzié, C.; Schweicher, G.; Salleo, A.; Geerts, Y.; Hecht, S.; et al. Optically Switchable Transistors by Simple Incorporation of Photochromic Systems into Small-Molecule Semiconducting Matrices. *Nat. Commun.* **2015**, *6*, 6330.

(16) Irie, M.; Fukaminato, T.; Matsuda, K.; Kobatake, S. Photochromism of Diarylethene Molecules and Crystals: Memories, Switches, and Actuators. *Chem. Rev.* **2014**, *114*, 12174−12277.

(17) Herder, M.; Schmidt, B. M.; Grubert, L.; Pätzel, M.; Schwarz, J.; Hecht, S. Improving the Fatigue Resistance of Diarylethene Switches. *J. Am. Chem. Soc.* **2015**, *137*, 2738−2747.

(18) Wang, Q.; Ligorio, G.; Diez-Cabanes, V.; Cornil, D.; Kobin, B.; Hildebrandt, J.; Nardi, M. V.; Timpel, M.; Hecht, S.; Cornil, J.; List-Kratochvil, E. J. W.; Koch, N. Dynamic Photoswitching of Electron Energy Levels at Hybrid ZnO/Organic Photochromic Molecule Junctions. *Adv. Funct. Mater.* **2018**, *28*, 1800716.

(19) Li, H.; Paramonov, P.; Bredas, J. L. Theoretical Study of the Surface Modification of Indium Tin Oxide with Trifluorophenyl Phosphonic Acid Molecules: Impact of Coverage Density and Binding Geometry. *J. Mater. Chem.* **2010**, *20*, 2630.

(20) Hotchkiss, P. J.; Li, H.; Paramonov, P. B.; Paniagua, S. A.; Jones, S. C.; Armstrong, N. R.; Brédas, J. L.; Marder, S. R. Modification of the Surface Properties of Indium Tin Oxide with Benzylphosphonic Acids: A Joint Experimental and Theoretical Study. *Adv. Mater.* **2009**, *21*, 4496−4501.

(21) Gliboff, M.; Li, H.; Knesting, K. M.; Giordano, A. J.; Nordlund, D.; Seidler, G. T.; Brédas, J. L.; Marder, S. R.; Ginger, D. S. Competing Effects of Fluorination on the Orientation of Aromatic and Aliphatic Phosphonic Acid Monolayers on Indium Tin Oxide. *J. Phys. Chem. C* **2013**, *117*, 15139−15147.

(22) Natan, A.; Kronik, L.; Shapira, Y. Computing Surface Dipoles and Potentials of Self-Assembled Monolayers from First Principles. *Appl. Surf. Sci.* **2006**, *252*, 7608−7613.

(23) Perdew, J. P.; Burke, K.; Ernzerhof, M. Generalized Gradient Approximation Made Simple. *Phys. Rev. Lett.* **1996**, *77*, 3865−3868.

(24) Blöchl, P. E. Projector Augmented-Wave Method. *Phys. Rev. B: Condens. Matter Mater. Phys.* **1994**, *50*, 17953−17979.

(25) Paniagua, S. A.; Hotchkiss, P. J.; Jones, S. C.; Marder, S. R.; Mudalige, A.; Marrikar, F. S.; Pemberton, J. E.; Armstrong, N. R. Phosphonic Acid Modification of Indium-Tin Oxide Electrodes: Combined XPS/UPS/Contact Angle Studies. *J. Phys. Chem. C* **2008**, *112*, 7809−7817.

(26) Paramonov, P. B.; Paniagua, S. A.; Hotchkiss, P. J.; Jones, S. C.; Armstrong, N. R.; Marder, S. R.; Brédas, J.-L. Theoretical Characterization of the Indium Tin Oxide Surface and of Its Binding Sites for Adsorption of Phosphonic Acid Monolayers. *Chem. Mater.* **2008**, *20*, 5131−5133.

(27) Wang, C.; Wang, H.-I.; Tang, W.-T.; Luo, C.-W.; Kobayashi, T.; Leu, J. Superior Local Conductivity in Self-Organized Nanodots on Indium-Tin-Oxide Films Induced by Femtosecond Laser Pulses. *Opt. Express* **2011**, *19*, 24286.

(28) Wood, C.; Li, H.; Winget, P.; Bredas, J. L. Binding Modes of Fluorinated Benzylphosphonic Acids on the Polar ZnO Surface and Impact on Work Function. *J. Phys. Chem. C* **2012**, *116*, 19125−19133.

(29) Gliboff, M.; Sang, L.; Knesting, K. M.; Schalnat, M. C.; Mudalige, A.; Ratcliff, E. L.; Li, H.; Sigdel, A. K.; Giordano, A. J.; Berry, J. J.; et al. Orientation of Phenylphosphonic Acid Self-Assembled Monolayers on a Transparent Conductive Oxide: A Combined NEXAFS, PM-IRRAS, and DFT Study. *Langmuir* **2013**, *29*, 2166−2174.

(30) Kresse, G.; Furthmüller, J. Efficiency of Ab-Initio Total Energy Calculations for Metals and Semiconductors Using a Plane-Wave Basis Set. *Comput. Mater. Sci.* **1996**, *6*, 15−50.

(31) Kresse, G.; Furthmüller, J. Efficient Iterative Schemes for Ab Initio Total-Energy Calculations Using a Plane-Wave Basis Set. *Phys. Rev. B: Condens. Matter Mater. Phys.* **1996**, *54*, 11169−11186.

(32) Paramonov, P. B.; Paniagua, S. A.; Hotchkiss, P. J.; Jones, S. C.; Armstrong, N. R.; Marder, S. R.; Brédas, J.-L. Theoretical Characterization of the Indium Tin Oxide Surface and of Its Binding Sites for Adsorption of Phosphonic Acid Monolayers Jean-Luc Bre Indium Tin Oxide (ITO) Is Currently the Most Widely Used Transparent Electrode in Organic Light-Emitting Devi. *Chem. Mater.* **2008**, *20*, 5131−5133.

(33) Mendive-Tapia, D.; Perrier, A.; Bearpark, M. J.; Robb, M. a; Lasorne, B.; Jacquemin, D. New Insights into the By-Product Fatigue Mechanism of the Photo-Induced Ring-Opening in Diarylethenes. *Phys. Chem. Chem. Phys.* **2014**, *16*, 18463−18471.

DOI: 10.1021/acsanm.9b00094
ACS Appl. Nano Mater. 2019, 2, 1102−1110

(34) Taylor, D. M.; de Oliveira, O. N.; Morgan, H. Models for Interpreting Surface Potential Measurements and Their Application to Phospholipid Monolayers. *J. Colloid Interface Sci.* **1990**, *139*, 508−518.
(35) Cornil, D.; Olivier, Y.; Geskin, V.; Cornil, J. Depolarization Effects in Self-Assembled Monolayers: A Quantum-Chemical Insight. *Adv. Funct. Mater.* **2007**, *17*, 1143−1148.
(36) Cornil, D.; Van Regemorter, T.; Beljonne, D.; Cornil, J. Work Function Shifts of a Zinc Oxide Surface upon Deposition of Self-Assembled Monolayers: A Theoretical Insight. *Phys. Chem. Chem. Phys.* **2014**, *16*, 20887−20899.
(37) Cornil, D.; Cornil, J. Work-Function Modification of the (1 1 1) Gold Surface upon Deposition of Self-Assembled Monolayers Based on Alkanethiol Derivatives. *J. Electron Spectrosc. Relat. Phenom.* **2013**, *189*, 32−38.
(38) Cornil, D.; Li, H.; Wood, C.; Pourtois, G.; Bredas, J. L.; Cornil, J. Work-Function Modification of Au and Ag Surfaces upon Deposition of Self-Assembled Monolayers: Influence of the Choice of the Theoretical Approach and the Thiol Decomposition Scheme. *ChemPhysChem* **2013**, *14*, 2939−2946.
(39) Heimel, G.; Romaner, L.; Brédas, J.-L.; Zojer, E. Interface Energetics and Level Alignment at Covalent Metal-Molecule Junctions: π-Conjugated Thiols on Gold. *Phys. Rev. Lett.* **2006**, *96*, 196806.
(40) Henkelman, G.; Arnaldsson, A.; Jónsson, H. A Fast and Robust Algorithm for Bader Decomposition of Charge Density. *Comput. Mater. Sci.* **2006**, *36*, 354−360.

DOI: 10.1021/acsanm.9b00094
ACS Appl. Nano Mater. 2019, 2, 1102−1110